International Journal of Nanomedicine

Dovepress
open access to scientific and medical research

Open Access Full Text Article

ORIGINAL RESEARCH

Construction of ROS-Responsive Hyaluronic Acid Modified Paclitaxel and Diosgenin Liposomes and Study on Synergistic Enhancement of Anti-Ovarian Cancer Efficacy

Ling Tang[1], Yu-Jia Wang[2], Yuan-Yuan Wang[2], Shu-Tong Li[3], Liang Kong[3], Xue-Tao Li[3], Ling-Ling Ma[1], Xiu-Xiu Liu[1]

[1]Department of Obstetrics and Gynecology, Affiliated Zhongshan Hospital of Dalian University, Dalian, People's Republic of China; [2]Department of Pharmacy, Affiliated Zhongshan Hospital of Dalian University, Dalian, People's Republic of China; [3]School of Pharmacy, Liaoning University of Traditional Chinese Medicine, Dalian, 116600, People's Republic of China

Correspondence: Ling-Ling Ma; Xiu-Xiu Liu, Department of Obstetrics and Gynecology, Affiliated Zhongshan Hospital of Dalian University, Dalian, People's Republic of China, Email 826269013@qq.com; 1225949002@qq.com

Purpose: Ovarian cancer is a fatal gynecologic malignancy with a high rate of abdominal metastasis. Chemotherapy still has a poor clinical prognosis for ovarian cancer patients, with cell proliferation and angiogenesis leading to invasion, migration, and recurrence. To overcome these obstacles, we constructed a novel HA-modified paclitaxel and diosgenin liposome (PEG-TK-HA-PDLPs) using two novel functional materials, DSPE-PEG_{2000}-HA and DSPE-PEG_{2000}-TK-PEG_{5000}, to specifically deliver the drugs to the tumor site in order to reduce OC cell proliferation and anti-angiogenic generation, thereby inhibiting invasion and migration.

Methods and Results: PEG-TK-HA-PDLPs were prepared by film dispersion, with ideal physicochemical properties and exhibits active targeting for enhanced cellular uptake. The ZIP synergy score for PTX and Dios was calculated using the online SynergyFinder software to be 3.15, indicating synergy. In vitro results showed that PEG-TK-HA-PDLPs were highly cytotoxic to ID8 cells, induced ID8 cell apoptosis, and inhibited ID8 cell migration and invasion. In vivo studies showed that PEG-TK-HA-PDLPs could prolong the circulation time in the blood, accumulate significantly in the tumor site, and effectively fight against angiogenesis with significant anti-tumor effects.

Conclusion: The production of PEG-TK-HA-PDLPs is an effective strategy for the treatment of OC.

Keywords: ovarian cancer, functional liposomes, paclitaxel, diosgenin, ROS-response, HA

Introduction

It is estimated that ovarian cancer (OC) accounted for 53.60% of its deaths in 2012 and 68.46% of its deaths in 2035 (an increase of 14.86%), making it the highest case-to-death ratio among gynecological cancers.[1,2] Currently, the main treatment for OC is surgical removal of the tumor followed by a combination of cisplatin and paclitaxel chemotherapy.[3,4] However, 80% of patients with advanced OC cancer will eventually relapse and have metastasis. In addition, relapsed patients develop resistance and severe side effects after receiving chemotherapy, and there has been little improvement in the survival of OC patients over the past three decades.[5–7] This underscores the need to provide novel treatments to address these side effects. To this end, new treatment options such as molecular targets are being investigated in OC clinical trials to combat OC.[8,9] Nevertheless, there are still some problems with these targeted drugs, such as insufficient circulation time of the drug in vivo and insignificant target specificity. Therefore, it is necessary to find more effective carrier systems that utilize nano-carriers to improve drug delivery efficiency and inhibit tumor cell proliferation and metastasis.

Received: 3 February 2024
Accepted: 23 May 2024
Published: 5 June 2024

Extensive peritoneal dissemination of OC cells can lead to inoperable metastatic lesions resulting in patient death, which is a major clinical problem in the treatment of OC.[10,11] When patients with ovarian cancer are diagnosed at an early stage, confined to one or both ovaries, less than 10% will die as a result.[12,13] Based on these studies suggest that metastasis is a major cause of high mortality from ovarian cancer and that inhibiting ovarian cancer metastasis is critical to the clinical management of this daunting disease.

Unlike normal tissues, the tumor microenvironment (TME) has interstitial high pressure and low convection due to resistance, making it impossible for chemicals to break through the body's blood and cellular barriers to reach the tumor site and to accumulate at the tumor site, which leads to the synthesis of a variety of stimulus-sensitive nanoparticles used for chemotherapy.[14] Biocompatible and biodegradable liposomes self-assembled from amphiphiles are representative carriers for anticancer drug delivery and may be the most promising tools for cancer chemotherapy.[15]

Suitable functional liposomes are useful tools to improve drug stability and bioavailability as well as targeted delivery to the tumor site.[16,17] However, the systematic delivery of targeted liposomes to solid tumors requires overcoming many physiological hurdles.[18] Ideally, functional liposomes should be able to respond to the specific physiological characteristics of TME (eg, weak acidity, high concentrations of glutathione (GSH) and reactive oxygen species (ROS), pH), and ROS-responsive nanoparticle drug delivery systems have been extensively studied.[19,20] Acetone-based thioketal (-SC$(CH_3)_2$S-, TK) is a ROS-responsive polymer that has been reported to enhance the efficiency of drug delivery in the TME and has great potential in anticancer.[21,22] When the tumor initiation, progression and peritoneal tumor spread was happened, the TME surrounding ovarian cancer cells was alter, such as produce both extracellular matrix molecule, hyaluronan (HA) and the HA receptor, CD44.[23] As the tumor begins to develop and the peritoneal tumor spreads, the TME surrounding the OC cells is altered, for example, by the production of the extracellular matrix molecule HA and the HA receptor CD44, which further promotes the motility of the ovarian cancer cells.[23] HA has a strong affinity for CD44, providing a targeting design and the invasive and metastatic processes of OC are closely associated with elevated levels of CD44.[24,25]

Paclitaxel (PTX) is a naturally occurring diterpene alkaloid from the bark and needles of *Taxus brevifolia*.[26] PTX has been widely used in gynecologic oncology therapy based on microtubule stabilization to inhibit cell cycle and induce apoptosis.[27] In addition, according to our previous study, PTX liposomes (PLPs) inhibited invasion and metastasis of OC and induced apoptosis in OC cells in ex vivo experiments.[16] diosgenin (Dios) is a typical natural product that is the active ingredient in some traditional Chinese medicines, such as *Dioscorea nipponica* and *Paridis rhizome*.[28] Several pharmacological tests have shown that Dios has antitumor, anti-inflammatory, antiviral and antifungal effects.[29,30] In addition, some studies suggest that Dios can reduce the viability and induced apoptosis of human ovarian cancer cells in a dose-dependent manner.[31]

In this study, we investigated a synergistic ROS-responsive liposome to enhance the targeting effect of OC TME. TK bonds on the liposome surface connect to PEG_{5000} to form a hydrated membrane that protects HA targeting to liposomes and passively targets OC sites through enhanced permeability and retention (EPR) effects, followed by oxidation and breakdown of TK to -SH within the ROS levels of tumor tissues (20–200 μM), which leads to rupture of the PEG hydrophilic outer shell layer of the liposomes, and exposure of HA to direct the liposomes to actively target the OC cell membrane surface.

Materials and Methods

Reagents and Cell Lines

Egg yolk phosphatidylcholine (EPC) and cholesterol (Chol) were obtained from Avanti Polar Lipids, Inc. (Alabaster, AL, USA). Paclitaxel was obtained from Meilun Co., Ltd. (Dalian, China). diosgenin was supplied by the Chengdu Derick Biotechnology Co., Ltd. (Chengdu, China). DSPE-PEG_{2000}-TK-PEG_{5000} and DSPE-PEG_{2000}-HA was purchase from Ruixi Biotechnology Co., Ltd. (Xian, China). Ki-67, EPO, VEGF, MMP-9 and TIE-2 antibodies were ordered from Biosynthesis Biotechnology Co., Ltd. (Beijing, China). 1.1-dioctadecyl-3,3,3,3-tetramethylindotricarbocyanine iodide (DiR) were supplied by Kaiji Biological Technology Development Co., Ltd. (Nanjing, China).

Human OC ID8 cells were acquired from the Institute of Basic Medical Science, the Chinese Academy of Medical Science (Beijing, China). Cells were cultured in DMEM medium (Meilun) with the supplement of 10% fetal bovine serum (FBS) (EallBio, Beijing, China), 100 U/mL penicillin and 100 μg/mL streptomycin at 37 °C in a humidified environment with 5% CO_2. Female BALB/c nude mice of weighing 20 ± 2 g were obtained from the Liaoning Changsheng Biotechnology Co., Ltd (Liaoning, China). Animal care and experimental protocols were performed in strict accordance with the guidelines of Liaoning University of Traditional Chinese Medicine Laboratory Animal Center and approved by the Laboratory Animal Ethics Committee of Liaoning University of Traditional Chinese Medicine (No. 210000420230203).

Preparation of Liposomes

PEG-TK-HA-PDLPs were prepared by membrane dispersion method. Briefly, EPC, Chol, PTX, Dios, DSPE-PEG_{2000}-HA and DSPE-PEG_{2000}-TK-PEG_{5000} were dissolved in methanol in the mass ratio of 22:4:0.45:0.24:2:2 in pear shaped vials and then dried by rotary evaporator at 37°C until a thin film was formed. The films were hydrated with 5 mL of phosphate buffer solution (PBS). The hydrated solution was placed in a centrifuge tube and sonicated on ice with a probe sonicator at 200 W for 10 min, and then the hydrated solution was passed through a 0.22 μm polycarbonate membrane three times to obtain PEG-TK-HA-PDLPs. Blank liposomes, PLPs, PDLPs and HA-PDLPs were also prepared following the same procedure. In the preparation of fluorescent liposomes, the fluorescent probe DiR was used instead of PTX and Dios.

Characterization of Liposomes

Particle size, polydispersity index (PDI) and zeta potential of the liposomes were measured using a Zetasizer Nano ZS90 instrument (Malvern Instruments). The morphology of PEG-TK-HA-PDLPs was observed by transmission electron microscopy (TEM, JEM-1200EX; JEOL). Liposomal suspension was subjected to elution with Sephadex G-100 to remove unloaded PTX and Dios, next that used to determine encapsulation efficiency (EE) by HPLC with an ultraviolet detector (LC- 2010AHT; Shimadzu). In addition, we determined the stability of HA-PDLPs and PEG-TK-HA-PDLPs over 21 days at 4 °C according to previous methods.[9] The release rate of PEG-TK-HA-PDLPs in vitro was determined using the dialysis method under sink conditions.[28] The EE% was calculated using the following formula: $EE\% = (W_{loaded}/W_{total}) \times 100\%$, where W_{loaded} and W_{total} represented the content of PTX or Dios in the liposomal suspension after and before passing through the Sephadex G-100 column, respectively.

Hemolysis Assay

Fresh blood from healthy rats was collected and mixed with heparin and stirred with a glass rod to remove fibrinogen, then washed with saline, and centrifuged at 1500 rpm for 20 minutes at 4°C. Erythrocyte pellets at the bottom were then washed with PBS until the upper liquid layer was yellow or colorless. The erythrocyte solution was subsequently formulated to a final concentration of 2% and mixed with the same volume of blank liposomes, PLPs, PDLPs, HA-PDLPs and PEG-TK-HA-PDLPs as samples and incubated at 37°C. Physiological saline solution and ddH_2O were treated as negative and positive control respectively. Photographs of the different formulation groups were taken and centrifuged at 1500 rpm for 10 min, and then the supernatants were collected and estimated using an enzyme-linked immunosorbent assay analyzer (HBS-1096A, DeTie, Nanjing, China) at a wavelength of 540 nm. Hemolysis rate (HR%) was calculated by the following formula: $HR\% = (A_{sam} - A_{neg})/(A_{pos} - A_{neg}) \times 100\%$, where A_{sam}, A_{neg}, and A_{pos} represent the absorbance values at 540 nm for the sample, negative control, and positive control, respectively.

Cellular Uptake and Targeting Effects in ID8 Cells

The uptake of different preparations by ID8 cells was assessed by flow cytometry and fluorescence microscopy. Coumarin was encapsulated in liposomes and used as a fluorescent probe. ID8 cells were incubated with different concentrations (1.5, 3 and 6 μM) of coumarin with coumarin liposomes (CLPs), HA-CLPs, PEG-TK-HA-CLPs, PEG-TK-HA-CLPs+NaOH and blank liposomes (Blank) for 2 h. The cells were incubated with 3 μM of coumarin for different time periods (1, 2 and 3 h). Subsequently, the cells were rinsed with cold PBS three times, harvested, centrifuged, and

resuspended in 500 μL cold PBS subjected to analysis the mean fluorescence intensity of coumarin using a FACScan flow cytometer (Becton Dickinson, San Jose, CA, USA).

To evaluate the intracellular distribution of the different liposomes, LPs-treated ID8 cells were incubated with the different formulations as described above. After incubation, cells were immobilized with 4% paraformaldehyde for 15 min, and then the nucleus was stained with DAPI for 10 mins in the darkness. Finally, different samples were image with a fluorescence microscope (Nikon Eclipse E800, Nikon, Tokyo).

Cellular Viability

The activity of ID8 cells treated with different preparations was assayed by sulforhodamine (SRB) staining and LIVE/DEAD staining, respectively. First, ID8 cells were incubated in 96-well plates (1.5×10^4 cells/well). After 24 h of incubation, the medium was replaced with PLPs, PDLPs, HA-PDLPs, PEG-TK-HA-PDLPs, PEG-TK-HA-PDLPs +NaOH and blank liposomes (Blank), respectively, with the concentration of PTX ranging from 0 to 10 μM, and the molar ratio of PTX to Dios was 2:1. After 48 h of incubation, cells were fixed with 10% ice-cold trichloroacetic acid for 1 h, then washed with distilled water and stained with 0.4% SRB for 20 minutes. After fixed with 10 mmol/L Tris Base buffer, the absorbance of samples was determined with an enzyme-linked immunosorbent assay reader at 540 nm wavelength. Cell survival was calculated as follows Survival = $(A_{treated}/A_{control}) \times 100\%$, where $A_{treated}$ and $A_{control}$ represent the absorbance values at 540 nm for treated and control cells, respectively. Live/dead cell staining experiments were performed considering the viability of ID8 cells cultured in different formulations. The living and dead cells of each group were stained with calflavin-AM and propyliodide (PI), respectively. ID8 cells were exposed to PLPs, PDLPs, HA-PDLPs, PEG-TK-HA-PDLPs, PEG-TK-HA-PDLPs+NaOH and blank liposomes (Blank), and at a PTX final concentration of 10μM. After 24 h of culture, according to the manufacturer's procedure, calcein-AM/PI double-stained working solutions were prepared and incubated in a humidified incubator for 30 min. The dye solution was then aspirated and washed three times with PBS, viewed using fluorescence microscopy to observe live and dead cells.

Synergy Determination with SynergyFinder

ID8 cells were seeded into 96-well plates (1.5×10^4 cells/well) and analyzed using the CCK-8 assay for 0 to 40 μM concentrations of both drugs, PTX and Dios. The concentration gradient of PTX or Dios was determined based on the IC_{50} value of the drug. The synergistic effect of the combination drugs (PTX and Dios) was analyzed at different concentrations (0 μM, 0.3125, 0.625 μM, 1.25 μM, 2.5 μM, 5 μM, 10 μM and 20 μM). Cell viability was measured by enzymolar as described above. Drug synergy scores were calculated using online SynergyFinder software (https://synergy-finder.fimmm.fi) to calculate the survival index and zero interaction potency (ZIP). ZIP synergy scores greater than 0 are synergistic and greater than 10 are strongly synergistic. Drug combination response heat maps were also developed to assess the therapeutic significance of the combination.

Measurement of Cell Proliferation

To evaluate the effect of varying preparations on cell proliferation, EDU staining assay was performed. Briefly, cells were seeded into each well of a 48-well plate and treated with PBS, PLPs, PDLPs, HA-PDLPs, PEG-TK-HA-PDLPs and PEG-TK-HA-PDLPs+NaOH with a final PTX concentration of 10 μM for 24 h, and then incubated with 20 mmol/L EDU for 2 h. The cells were fixed with paraformaldehyde for 20 min and then the nucleus was stained with DAPI in the dark for 10 min, EDU-positive cells of different formulations were analyzed.

Hoechst/PI Double Staining Assay

Hoechst DNA staining and propidium iodide (PI) staining were used to detect the apoptosis of ID8 cells induced by different formulations. Cells were seeded in 48-well plates at a density of 1×10^4 cells/well and treated with PBS, PLPs, PDLPs, HA-PDLPs, PEG-TK-HA-PDLPs and PEG-TK-HA-PDLPs+NaOH with a final PTX concentration of 10 μM for 24 h. Hoechst 3342 (1 μg/mL) and PI (1 μg/mL) were added for 30 min and 10 min, respectively. The PI-positive cells were observed to measure cell apoptosis and necrosis using a fluorescence microscopy. The cell apoptosis rate was

calculated by the following equation: cell apoptosis rate = $(A_{pos}/A_{tot}) \times 100\%$, where A_{pos} and A_{tot} represent the number of PI-positive cells and the total number of cells, respectively.

Wound Healing Assay

To evaluate the migration ability of ID8 cells with treatment of different formulations, a wound healing assay was performed. ID8 cells were plated in 6-well plates (2×10^5 cells/well) and cultured at 37°C until 80~90% confluent. Use a 20 μL sterile pipette to make a wound along the bottom of the petri dish to create a scratch. The plates were washed with PBS to clear the floating cells and then the varying formulations were added into the medium at a final concentration of 10 μM PTX. Cells were observed at different time points (0, 12 and 24 h) and wound closure was observed with an inverted microscope (XDS-1B, Chongqing Photoelectric Co., Ltd., Chongqing, China). Calculation formula of wound healing rate: Healing rate = $(A_{0h}\text{-}A_{xh})/A_{0h} \times 100\%$, where A_{0h} and A_{xh} represent the wound area measure at 0 h and 12 h or 24 h, respectively.

Inhibition of ID8 Cells Invasion and Migration

Cell invasion and migration assays were performed using The Transwell chambers. The upper chamber was injected with 200 μL of FBS-free medium containing ID8 cells at a density of 5×10^4 cells/well for the invasion assay and 1.5×10^4 cells/well for the migration assay. The lower chamber was filled with 600 μL of medium containing 5% FBS as the invasion or migration attractant. Then, different formulations were added to the upper chamber at a PTX final concentration of 10 μM and culture medium was used as the control group. The chamber membranes were pre-coated with diluted Matrigel for invasion assay. After 24 h of incubation, the cell culture medium was discarded and the upper cell chamber was flushed with PBS, then fixed with 4% paraformaldehyde for 15 min and stained with crystal violet for 30 min. Finally, the migrating or invading cells were counted and photographed under an inverted microscope.

Real-Time Imaging in vivo

The distribution and targeting effects of various formulations in tumor-bearing mice was assessed by a noninvasive imaging system. The nude mouse model bearing allograft tumors of OC was established based our previous research. In brief, 1.5×10^6 cells/200 μL FBS-free medium of ID8 cells were injected into right forelimb of BALB/c nude mice. When the tumors reached approximately 400 mm^3 in volume, the tumor-bearing mice were randomly divided into four groups. Normal saline (Blank), free DiR, DiR-LPs, or PEG-TK-HA-DiR-LPs was injected into the nude mice at a DiR dose of 2 μg per mouse through the tail vein. After the mice were anesthetization with isoflurane and then bioluminescence signals of the mice were acquired using a Kodak multimodal imaging system (Carestream Health, Inc., USA) at 6, 12, 36, 48 and 72 h.

Evaluation of Efficacy in vivo

Tumor-bearing mice were inoculated as described above, and when the tumor volume reached approximately 300 mm^3, the tumor-bearing mice were randomly divided into five groups, each of which was injected with Free PTX/Dios, PDLPs, HA-PDLPs, PEG-TK-HA-PDLPs, or normal saline (Blank) by tail vein at a dosage of 5 mg/kg PTX. Tumor size was measured every other day after the first injection, and tumor volumes were calculated according to the formula: $V = \text{length} \times \text{width}^2/2\ (mm^3)$. Tumorinhibitoryrate $= 100\% - (V_{drug}/V_{saline}) \times 100\%$, where V_{drug} and V_{saline} are the tumor volumes after treatment with drug and normal saline, respectively, and the body weights of mice were measured six times to assess the safety of different formulations. Tumor-bearing mice were sacrificed by cervical dislocation and sections of tumor tissue, heart, liver, spleen, lungs, and kidneys were stained with hematoxylin and eosin (H&E) to further assess the safety of the different preparations. H&E staining and terminal deoxynucleotidyl transferase dUTP nick end labeling (TUNEL) assay were used to compare the tumor-damaging and apoptosis-inducing effects of different formulations in vivo. Ki-67 antibody was used to detect the proliferation status of tumor tissues. In addition, the expression of angiogenesis-related proteins, including EPO, VEGF, MMP-9, and TIE-2, was detected by immunofluorescence.

Statistical Analysis

Statistical analysis was performed using GraphPad Prism 9.0 and SPSS 19.0 software. Data were externally presented as mean ± standard deviation (SD). Differences between groups were analyzed by one-way ANOVA, and $P<0.05$ was considered statistically significant.

Results

Characterization of Liposomes

Table 1 listed the EE% of the various liposomes and Table 2 listed the physical properties of the various liposomes, including values related to particle size, PDI, and zeta potential. As shown in Figure 1A–D, PEG-TK-HA-PDLP has a more homogeneous size and more stable dispersion than HA-PDLP. The particle size, zeta potential and PDI of PEG-TK-HA-PDLPs were 111.79±4.50 nm, −1.47±0.12 and 20.73±1.93, respectively, and the EE% of PTX and Dios in PEG-TK-HA-PDLPs were 93.39±1.09% and 84.97±4.27%, respectively (Figure 1G–I). The morphology of PEG-TK-HA-PDLPs was characterized by TEM, which showed that the PEG-TK-HA-PDLPs were homogeneous and smooth spherical with a hydrophobic core having a weakly hydrophilic outer shell (Figure 1E). In our study, the hemolysis caused by different formulations was assessed. In Figure 1F and J, compared with positive control, all liposome groups were significant decreased the hemolysis rate, due to the formation of spherical LPs decreased the interaction surface area and kept the erythrocyte membranes undisturbed to avoiding hemolysis. In the stability experiments, the EE% of PEG-TK-HA-PDLPs was greater than 80% in 21 days and higher than that of HA-PDLPs, demonstrating that the incorporation of the hydrophilic material DSPE-PEG_{2000}-TK-PEG_{5000} improved the stability of the liposomes (Figure S1). The in vitro release results showed that the addition of DSPE-PEG_{2000}-TK-PEG_{5000} enabled the drug to achieve a slow release effect, better protecting the drug to reach the tumor site and releasing the drug at a greater rate in a Ros-responsive environment (Figure S2).

Cellular Uptake

As shown in Figure 2, the targeting effect of different formulations was demonstrated by the fluorescence images captured by microscope. We can observe that the fluorescence intensity of the drug-treated group increases gradually with the passage of time and the increase of drug content subsequently. It can also be noted that the intracellular fluorescence intensity of HA-CLPs and PEG-TK-HA-CLPs+NaOH is almost the same and stronger than that of CLPs and PEG-TK-HA-CLPs. Quantitative assessment by flow cytometry showed that the fluorescence intensity was in the order of PEG-TK-HA-CLPs-NaOH > HA-CLPs > PEG-TK-HA-CLPs > CLPs > Blank with time and increasing drug content (Figure 3). The results showed that the addition of HA significantly increased drug uptake by ID8 cells, and the DSPE-PEG_{2000}-TK-PEG_{5000} bond in PEG-TK-HA-CLPs was able to protect the targeting molecule HA. With longer

Table 1 Encapsulation Efficiency of Varying Liposomes (n=3)

Liposomes	PTX EE%	DIO EE%
PLPs	95.08±2.11	–
PDLPs	90.82±4.59	92.74±3.57
HA-PDLPs	94.98±3.35	95.66±1.36
PEG-TK-HA-PDLPs	93.39±1.09	84.97±4.27

Table 2 Particle Size, PDI Value and Zeta Potential of Liposomes (n=3)

Liposomes	Size (nm)	PDI (%)	Zeta (mV)
PEG-TK-HA-PDLPs	111.79±4.50	20.73±1.93	−1.47±0.12
PEG-TK-HA-PDLPs+NaOH	83.38±4.70	24.43±1.53	−2.33±0.15

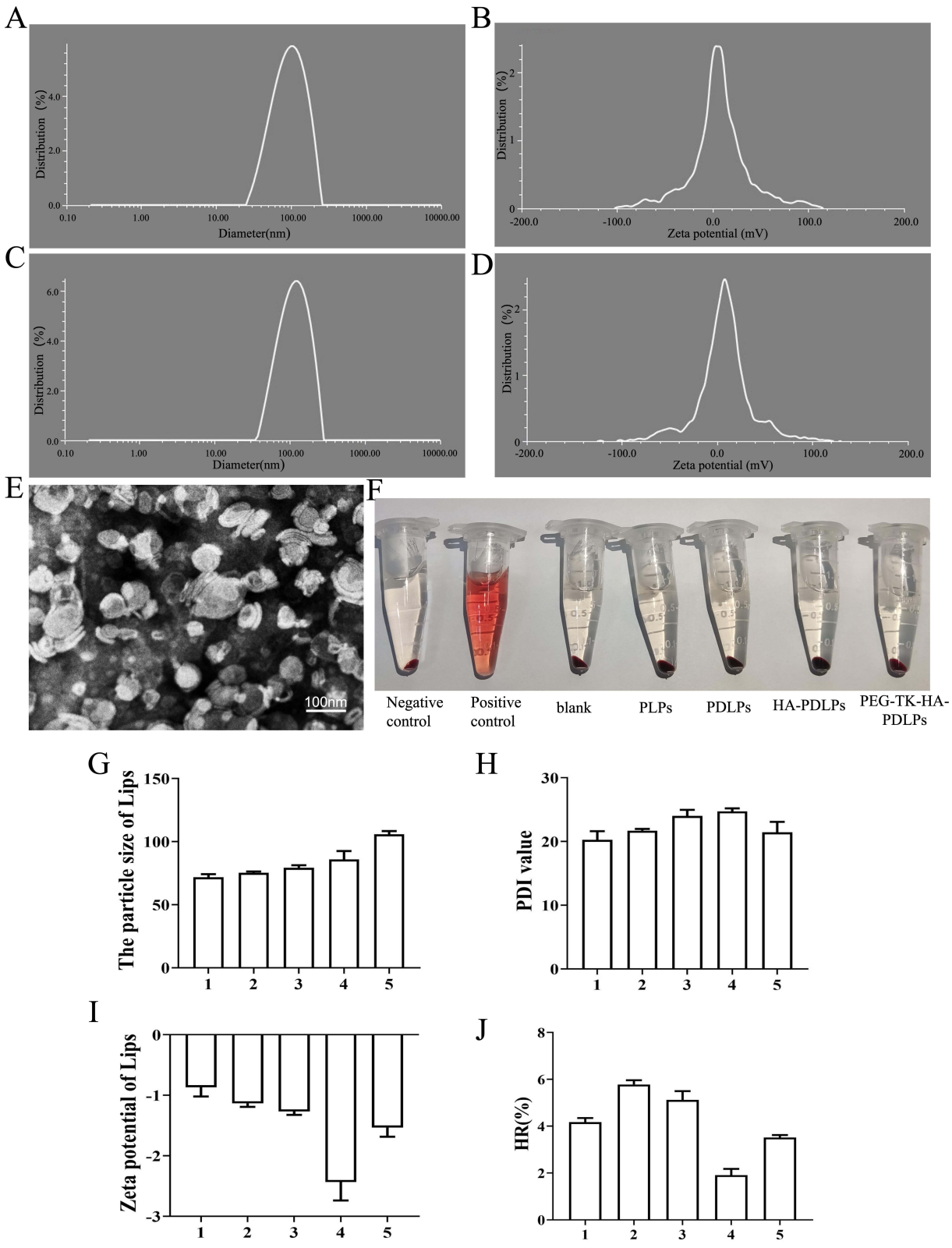

Figure 1 Characterization of the varying liposomes. (**A**) Representative images of particle sizes of HA-PDLPs; (**B**) Representative images of zeta potential of HA-PDLPs; (**C**) Representative images of particle sizes of PEG-TK-HA-PDLPs; (**D**) Representative images of zeta potential of PEG-TK-HA-PDLPs; (**E**) TEM image of PEG-TK-HA-PDLPs;, scale bar = 100 nm; (**F**) Changes in different preparations incubated for 2h at 37°C in 2% red cells suspension; (**G**) Quantitative analysis of particle size of the varying formulations; (**H**) Quantitative analysis of PDI value of the varying formulations; (**I**) Quantitative analysis of zeta potential of the varying formulations; (**J**) Haemolysis rate; 1. Blank, 2. PLPs, 3. PDLPs, 4. HA-PDLPs, 5. PEG-TK-HA-PDL.

https://doi.org/10.2147/IJN.S455942 DovePress

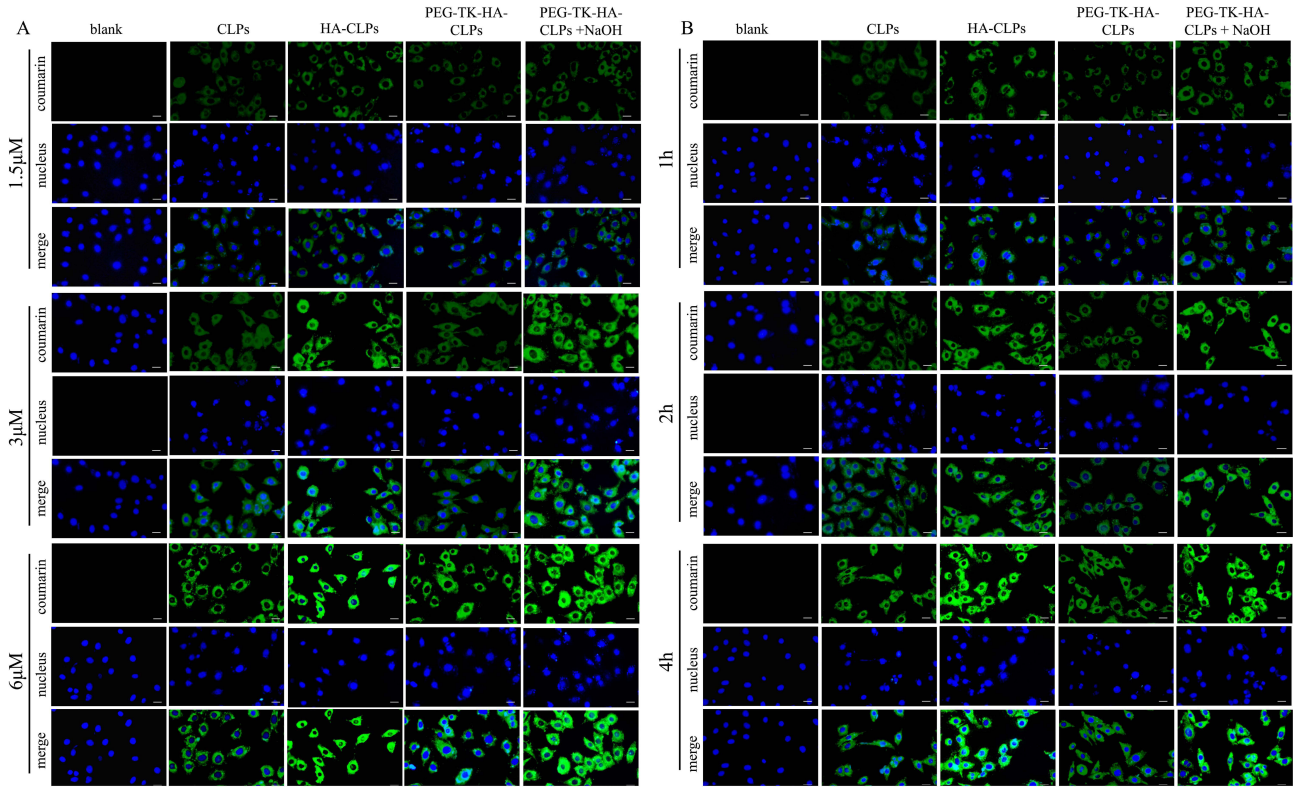

Figure 2 Cellular uptake and targeting effects in ID8 cells treated with the varying formulations by microscopy. (**A**) Cellular uptake and distribution of ID8 cells treated with the various of formulations at different concentrations, scale bar = 50 μm; (**B**) Cellular uptake and distribution of ID8 cells treated with the various of formulations at a series of time points, scale bar = 50 μm; All data are presented as mean ± SD (n = 3). *P < 0.05, **P < 0.01, ***P < 0.001, ****P < 0.0001.

incubation time or higher drug concentration, the fluorescence of HA-CLPs and PEG-TK-HA-CLPs+NaOH was almost the same, which was consistent with the results of fluorescence microscopy (Figure 3C and D).

Cell Viability

To assess the inhibitory effect of different preparations on ID8 cells, SRB assay and LIVE/DEAD staining assay were performed as shown in Figure 4. Cytotoxic effects of different formulations on ID8 cells are presented in Figure 4A and B. After 48 hours of incubation, the cytotoxicity of the blank group was negligible, which proves that the membrane material we used is safe. In addition, the inhibitory effect of different liposomal groups on ID8 cell growth was dose-dependent with increasing PTX concentration. Among these different formulations, PEG-TK-HA-PDLPs+NaOH showed the strongest cytotoxicity. IC_{50} values for PLPs, PDLPs, HA-PDLPs, PEG-TK-HA-PDLPs and PEG-TK-HA-PDLPs+NaOH were 2.03 ±0.54, 1.60±0.27, 0.99±0.28, 1.59±0.17, and 0.40±0.03 μM, respectively. The live/dead status of ID8 cells as affected by the different formulations was then directly assessed using the Calcein-AM/PI live/dead probe. In Figure 4D, there were almost no dead cells in the blank group, while PEG-TK-HA-PDLPs+NaOH showed the strongest killing effect in all groups.

Synergy Determination with SynergyFinder

The above in vitro cytotoxicity results have shown that the addition of Dios enhanced the cytotoxicity of PTX on ID8 cells. The ZIP synergy score was determined using the new concentration gradient and inhibition index (Figure 4C). The results showed that PTX and Dios synergistically enhanced cytotoxicity in ID8 cells (ZIP synergy score=3.15), with the white rectangle indicating the region of maximum synergy.

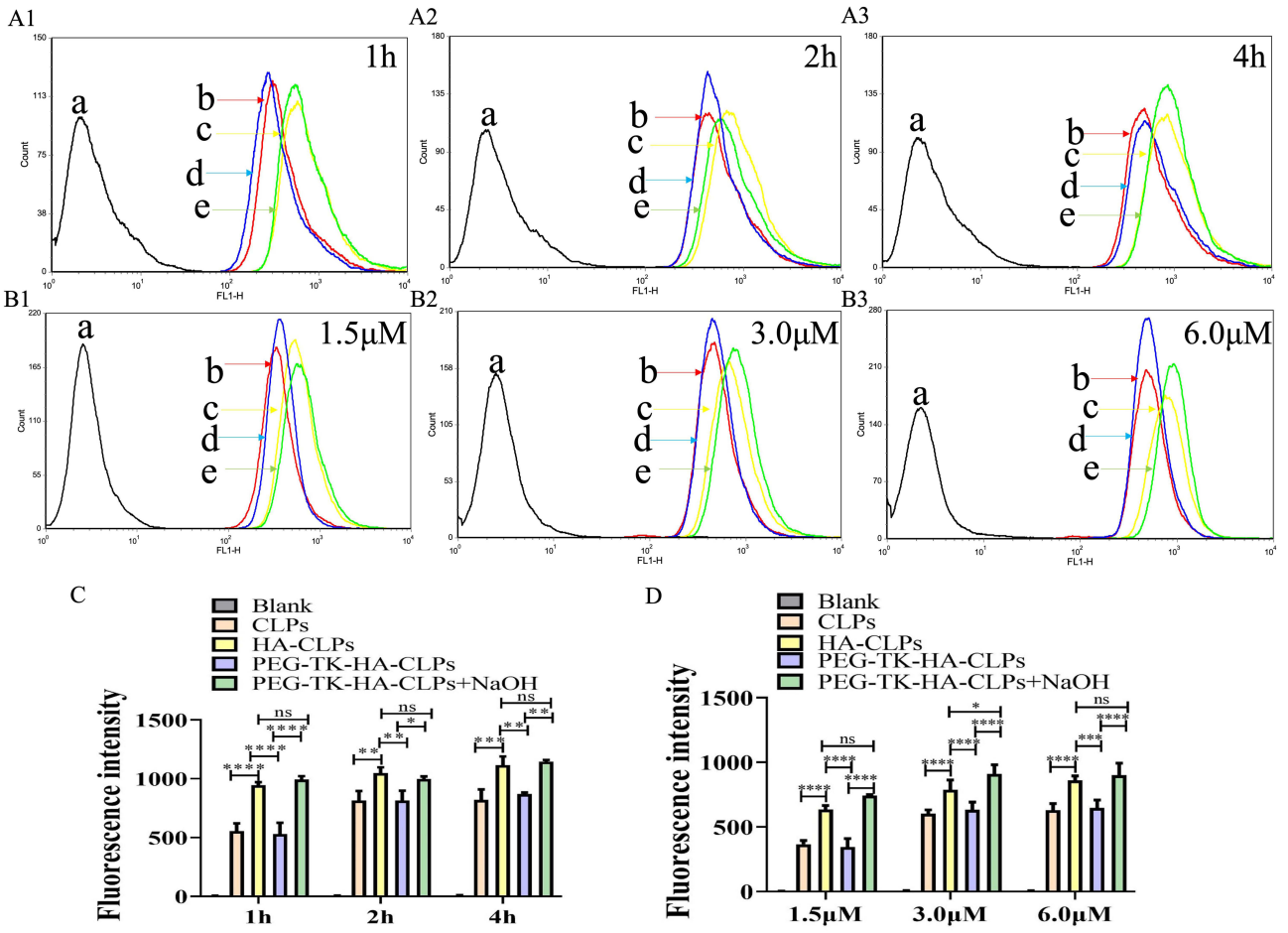

Figure 3 Cellular uptake and targeting effects in ID8 cells treated with the varying formulations by flow cytometry. (**A1**–**A3**) Cellular uptake of varying formulations for 1h, 2h, 4h; (**B1**–**B3**) Cellular uptake of varying formulations for 1.5 μM, 3 μM, 6 μM. (**C**) Quantitative analysis of fluorescence intensity of ID8 cells treated with the various of formulations at a series of time points; (**D**) Quantitative analysis of fluorescence intensity of ID8 cells treated with the various of formulations at different concentrations; a. Blank, b. CLPs, c. HA-CLPs, d. PEG-TK-HA-CLPs, e. PEG-TK-HA-CLPs + NaOH. All data are presented as mean ± SD (n = 3). **P* < 0.05, ***P* < 0.01, ****P* < 0.001, *****P* < 0.0001.

Inhibition of Proliferation in vitro

EDU staining assay was carried out to study the inhibitory effect on the proliferation of ID8 cells after treatment with different preparations. As shown in Figure 5A–C, the EDU assay results indicated that HA-PDLPs and PEG-TK-HA-PDLPs+NaOH significantly inhibited EDU-positive cells compared with Blank, which was consistent with the cell viability assay results.

Hoechst/PI Double Staining Assay

The role of apoptosis in different liposomal formulations-induced cell death was examined by Hoechst/PI double staining. As shown in Figure 5B, Hoechst-stained nuclei (blue) represent total cells and PI-positive cells (red) represent apoptotic cells. Fluorescence microscopy showed that cells exposed to HA-PDLPs and PEG-TK-HA-PDLPs+NaOH appeared to have the most PI-positive cells, suggesting that both sets of formulations have pro-apoptotic activity. Compared with the Blank group, the apoptosis ratio of ID8 cells treated with PLPs, PDLPs, HA-PDLPs, PEG-TK-HA-PDLPs and PEG-TK-HA-PDLPs+NaOH increased from (6.52±1.66)% in the control group to (12.00±1.91)%, (14.69±3.81)%, (28.32±4.06)%, (15.40±1.35)% and (28.50 ±8.00)% (Figure 5D).

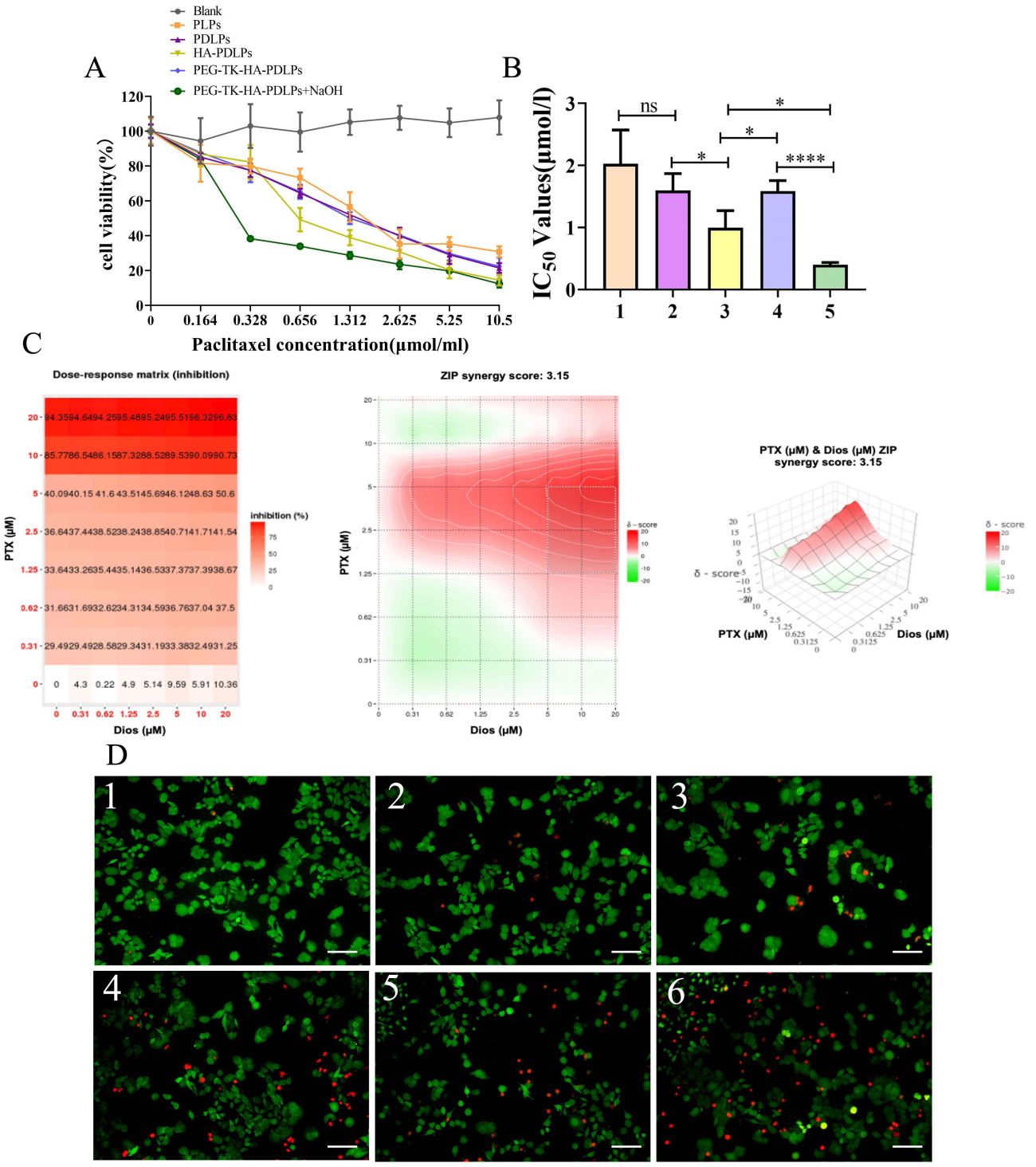

Figure 4 Evaluation of safety and cell viability of different formulations. (**A**) SRB assay for cytotoxicity of different formulations in ID8 cells; (**B**) IC50 values of different formulations. 1. PLPs, 2. PDLPs, 3. HA-PDLPs, 4. PEG-TK-HA-PDLPs; 5. PEG-TK-HA-PDLPs + NaOH; (**C**) Heatmaps of drug combination responses. (**D**) Results of LIVE/DEAD staining of ID8 cells after administration of different formulations, scale bar = 50 μm. 1. Blank, 2. PLPs, 3. PDLPs, 4. HA-PDLPs, 5. PEG-TK-HA-PDLPs; 6. PEG-TK-HA-PDLPs + NaOH; All data are presented as mean ± SD (n = 3). *P < 0.05, ****P < 0.0001.

Wound Healing Assay

Figure 6A visually shows the inhibitory effect of different formulations on ID8 cell migration. The results of wound healing experiments showed that the cell scratch healing rate was (84.65±0.06)% after 24 h without any intervention, and

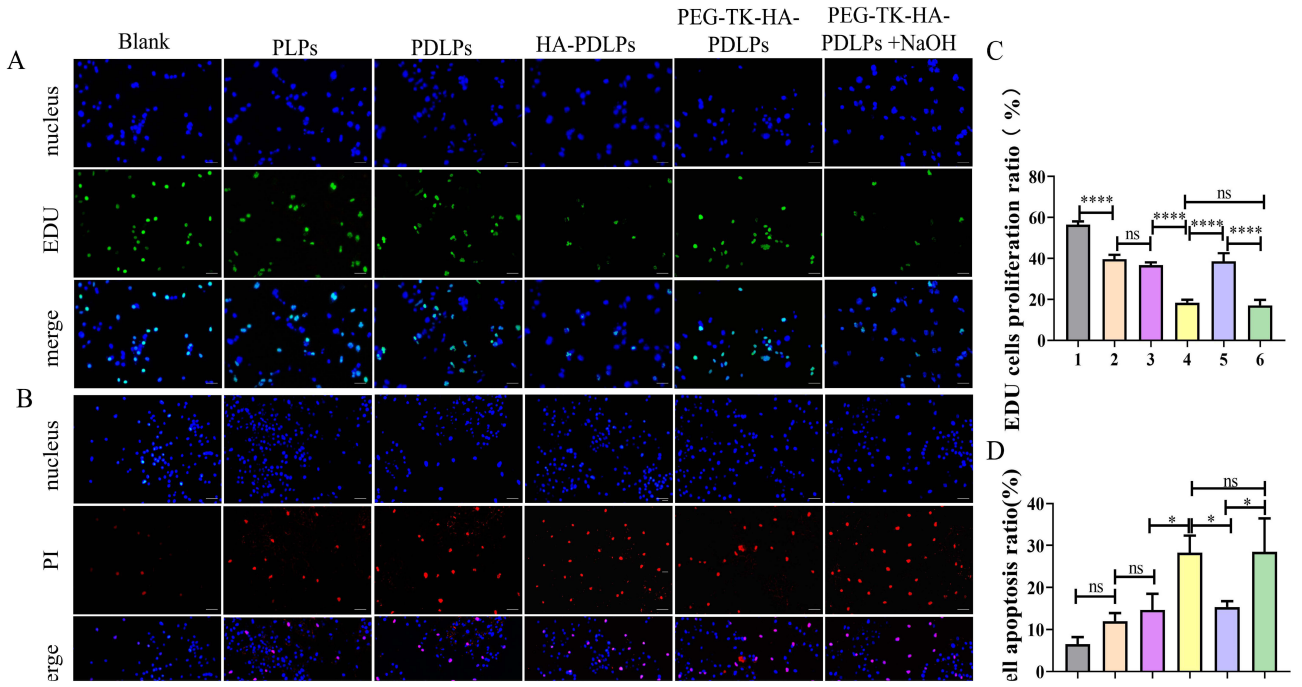

Figure 5 Inhibit the proliferation of tumor cells and promote the apoptosis of tumor cells after treatments with the varying formulations. (**A**) EDU staining assay to detect the effect of different formulations on proliferation in ID8 cells, scale bar = 25 μm; (**B**) Hoechst/PI double staining assay to detect the effect of different formulations on apoptosis in ID8 cells, scale bar = 25 μm; (**C**) EDU positive cells rate; (**D**) Apoptosis cells rate. 1. Blank, 2. PLPs, 3. PDLPs, 4. HA-PDLPs, 5. PEG-TK-HA-PDLPs; 6. PEG-TK-HA-PDLPs + NaOH. All data are presented as mean ± SD (n = 3). *P < 0.05, ****P < 0.0001.

the wound healing rates of ID8 in the PLPs, PDLPs and PEG-TK-HA-PDLPs groups were (75.01±5.57)%, (69.19 ±1.64)% and (69.90±2.44)%, respectively, which was slightly lower than that of the Blank group. The cell healing ability of HA-PDLPs and PEG-TK-HA-PDLPs+NaOH-treated groups was (24.08±2.88)% and (22.56±2.67)%, respectively, which was much lower than that of the blank group, suggesting that they could effectively inhibit the cell migration of ID8 (Figure 6D).

Inhibition of ID8 Cells Invasion and Migration

First, the migration ability of different formulations was analyzed by wound healing test. The results showed that the ability of PEG-TK-HA-PDLPs+NaOH to inhibit migration was significantly higher, and then we performed a Transwell assay to further investigate the inhibitory effects on invasion and migration after treatment with different formulations. The results of Transwell invasion assay showed that PEG-TK-HA-PDLPs+NaOH significantly reduced the number of infiltrated cells, and the relative invasion rate was (14.66±4.54)% (Figure 6B and E). Figure 6C and F show the inhibitory effect of different formulations on ID8 cell migration, where PEG-TK-HA-PDLPs+NaOH had the strongest inhibitory effect on migration with a relative migration rate of (21.81±2.34)% (Figure 6F), which is consistent with the wound healing results.

Fluorescence Imaging in vivo

We used a fluorescence imaging system to inject varying formulations into the tail vein of nude mice bearing ID8 tumor cells to explore targeting and circulation time at the tumor site. As shown in Figure 7, a slight fluorescent signal was detected in the Free DiR group; on the contrary, a strong fluorescent signal was clearly observed at different time points within 72 h after intravenous injection of PEG-TK-HA-DiR-LPs. The increased accumulation at the tumor site can be attributed to the DSPE-PEG_{2000}-TK-PEG_{5000} linkage, allowing for the generation of the EPR effect as well as more effective specificity of HA with tumor cells.

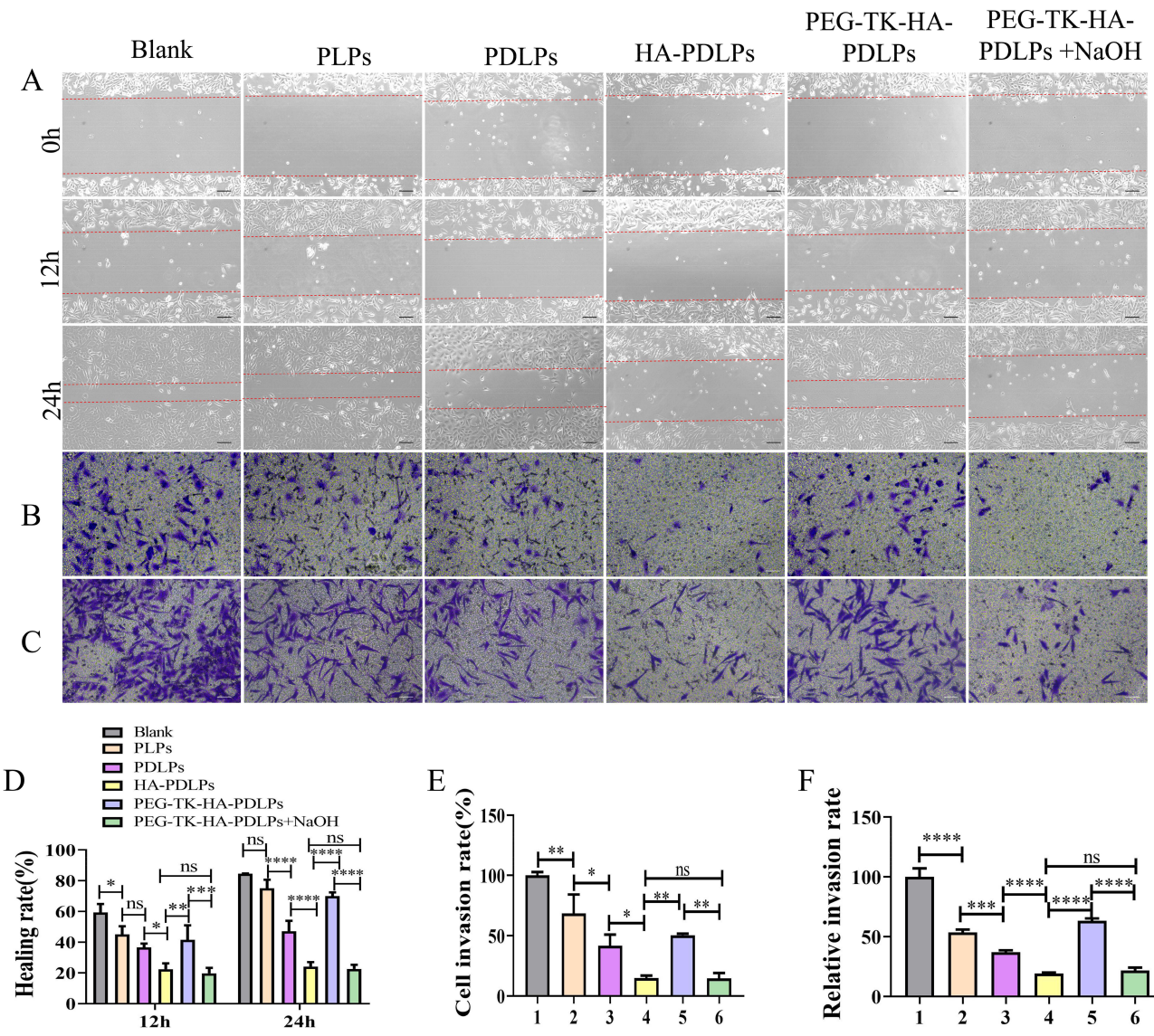

Figure 6 Effect of different formulations on the migratory and invasive capacity of ID8 cells. (**A**) Micrographs of migration ability of ID8 cells in each group, scale bar = 50 μm; (**B**) Micrographs of cell invasion ability assay for each group, scale bar = 100 μm; (**C**) Micrographs of cell migration ability assay for each group, scale bar = 100 μm; (**D**) Statistical analysis of cell healing rate in each group; (**E**) Cell relative invasion rate; (**F**) Cell relative migration rate. 1. Blank, 2. PLPs, 3. PDLPs, 4. HA-PDLPs, 5. PEG-TK-HA-PDLPs; 6. PEG-TK-HA-PDLPs + NaOH. All data are presented as mean ± SD (n = 3). **P* < 0.05, ***P* < 0.01, ****P* < 0.001, *****P* < 0.0001.

Antitumor Efficacy in vivo

In order to assess the antitumor effects of the different formulations in vivo, body weight changes, tumor inhibitory rate, safety, and inhibition of tumor metastasis in treated tumor-bearing mice were evaluated. As shown in Figure 8A, there was no significant weight loss in the PEG-TK-HA-PDLPs compared to the Blank group. Compared with the Blank group, different formulations inhibited tumor growth to different degrees, with PEG-TK-HA-PDLPs having the most significant inhibitory effect on tumor growth (Figure 8B). As shown in Figure 8C, the tumor inhibition rate of free PTX/Dios was (17.69±7.09)%, PDLPs was (38.63±9.04)%, HA-PDLPs was (58.32±12.02)%, and PEG-TK-HA-PDLPs was (70.84±15.03)% on the day 22 after incubation. Figure 8D shows the H&E-stained organs of the tumor-bearing mice, which showed no significant damage to the organs in all groups of mice. In addition, H&E staining of tumor tissue sections showed cell necrosis and structural disruption of tumor tissues in the PEG-TK-HA-PDLPs group (Figure 9A). Furthermore, to detect apoptotic and proliferating cells in tumor tissues, TUNEL assay and Ki-67 antibody staining were performed, respectively. The results of TUNEL assay showed that the highest level of apoptosis was observed in tumor

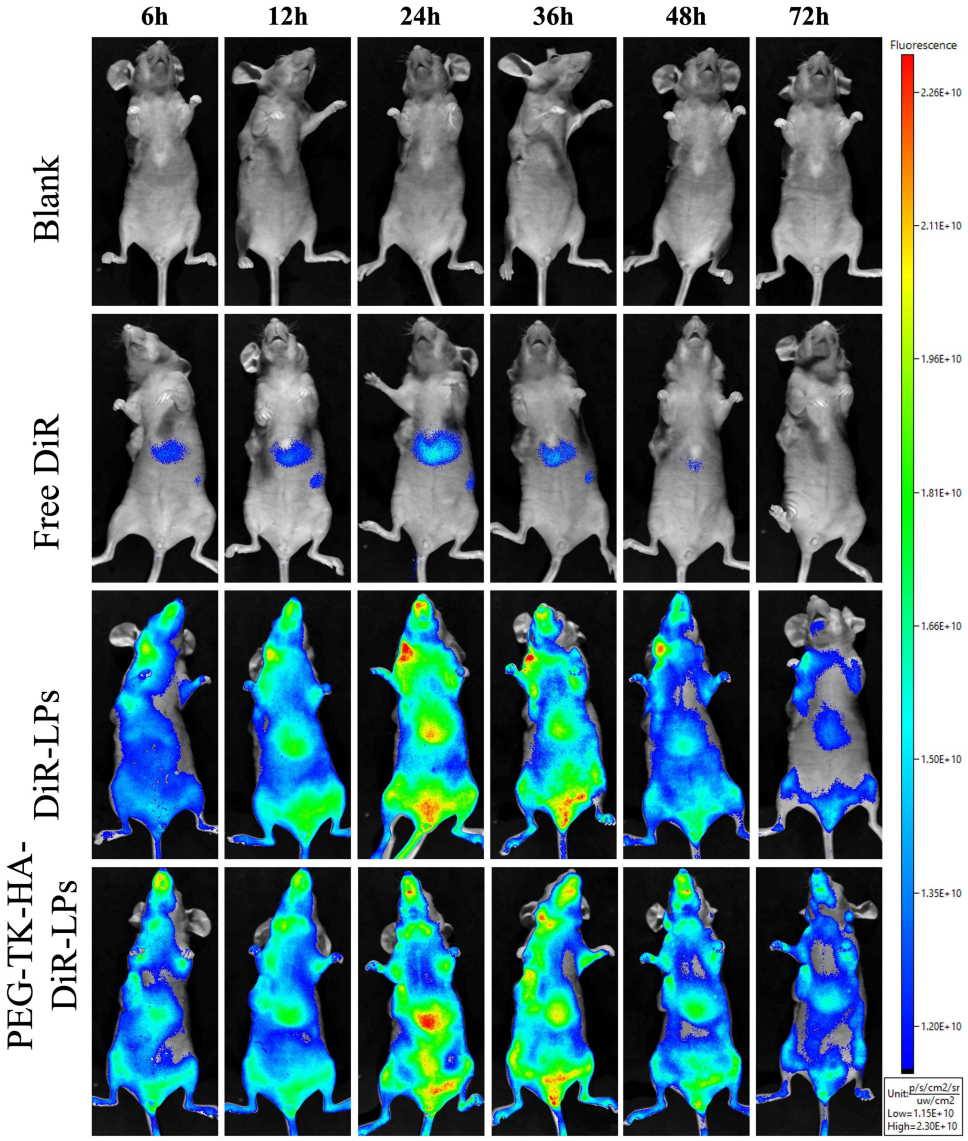

Figure 7 Real-time imaging observation of tumor bearing mice treated with varying formulations in vivo.

cells in the PEG-TK-HA-PDLPs group (Figure 9B). As shown in Figure 9C, the number of Ki-67-positive cells was significantly reduced after PEG-TK-HA-PDLPs treatment, which was opposite to the apoptotic trend detected by TUNEL. Finally, key angiogenesis-related proteins that support tumor metastasis were detected by immunofluorescence staining, including EPO, VEGF, MMP-9, and TIE-2. As shown in Figure 10A, the relative fluorescence intensity of angiogenesis-related proteins was attenuated to varying degrees after treatment with various formulations compared with the Blank group. A semiquantitative evaluation by ImageJ software analysis showed that the relative fluorescence intensity rankings were: Free PTX/Dios > PDLPs > HA-PDLPs > PEG-TK-HA-PDLPs (Figure 10B–E).

Discussion

Currently, the standard of treatment for patients with OC still involves surgery and platinum-based chemotherapy.[32] Although some patients respond to chemotherapy, most patients die from tumor metastasis and recurrence, as well as severe systemic toxicity caused by poorly targeted chemotherapeutic agents.[33] Therefore, there is a necessity to develop new delivery strategies to improve the therapeutic efficacy of OC. Incorporation of response molecules into targeted liposomes enables target specificity and sustained drug release, resulting in improved therapeutic efficacy and reduced

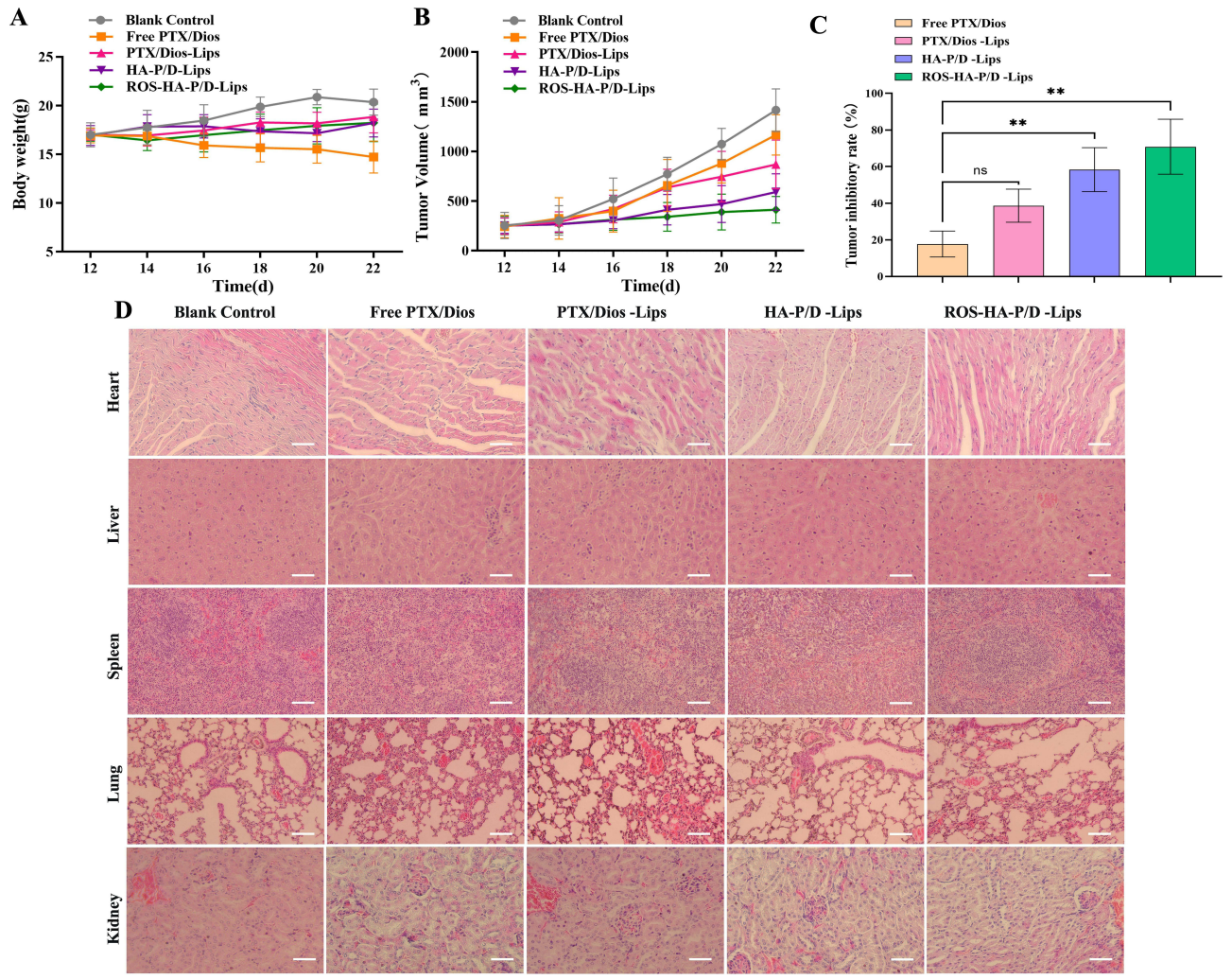

Figure 8 Safety inspection. (**A**) Changes in body weight during treatment. (**B**) Changes in tumor volume. (**C**) Tumor inhibition rate. (**D**) H&E staining results of organs. Scale bar, 25 μm. Data are presented as mean ± SD (n = 3), $^{**}P<0.01$.

drug toxicity. Hypoxia, a unique feature of cancer, dramatically alters ROS within tumor tissues, resulting in much higher levels of ROS in cancer cells than in normal tissues, and ROS-sensitive approaches that are more tumor-specific are particularly promising for increasing the exposure of cancer cells to therapeutic molecules.[34] The overall goal of the study is to develop a drug delivery platform that enhances OC cell target specificity and prolongs drug circulation time in the vivo to effectively inhibit OC cell invasion and metastasis. Herein, the ROS-sensitive (TK) is used as a stimulus and protects our newly designed targeting liposomes to reach the tumor site and then expose the HA to achieve better long-circulating action and specificity.

In this study, HA-targeting ligands were modified on the surface of liposomes and DSPE-PEG_{2000}-TK-PEG_{5000} was attached to the outer layer of liposomes, which improved the targeting synergistic delivery effect of liposomes, and the combined use of PTX and Dios in liposomes synergistically enhanced cytotoxicity against ID8 cells, which resulted in a more potent inhibitory effect on the invasive metastasis of ID8 cells. PEG-TK-HA-PDLPs were successfully prepared by thin film dispersion. When PEG-TK-HA-PDLPs were delivered to the tumor site, the ROS-sensitive (TK) was broken down to -SH, and the HA-PDLPs were exposed and had a strong binding capacity to the CD44 receptor overexpressed in the OC. The negatively charged surface of this functional liposome, which had a high drug loading capacity, good biocompatibility, and a suitable particle size, was conducive to the EPR effect to facilitate its tumor tissue accumulation

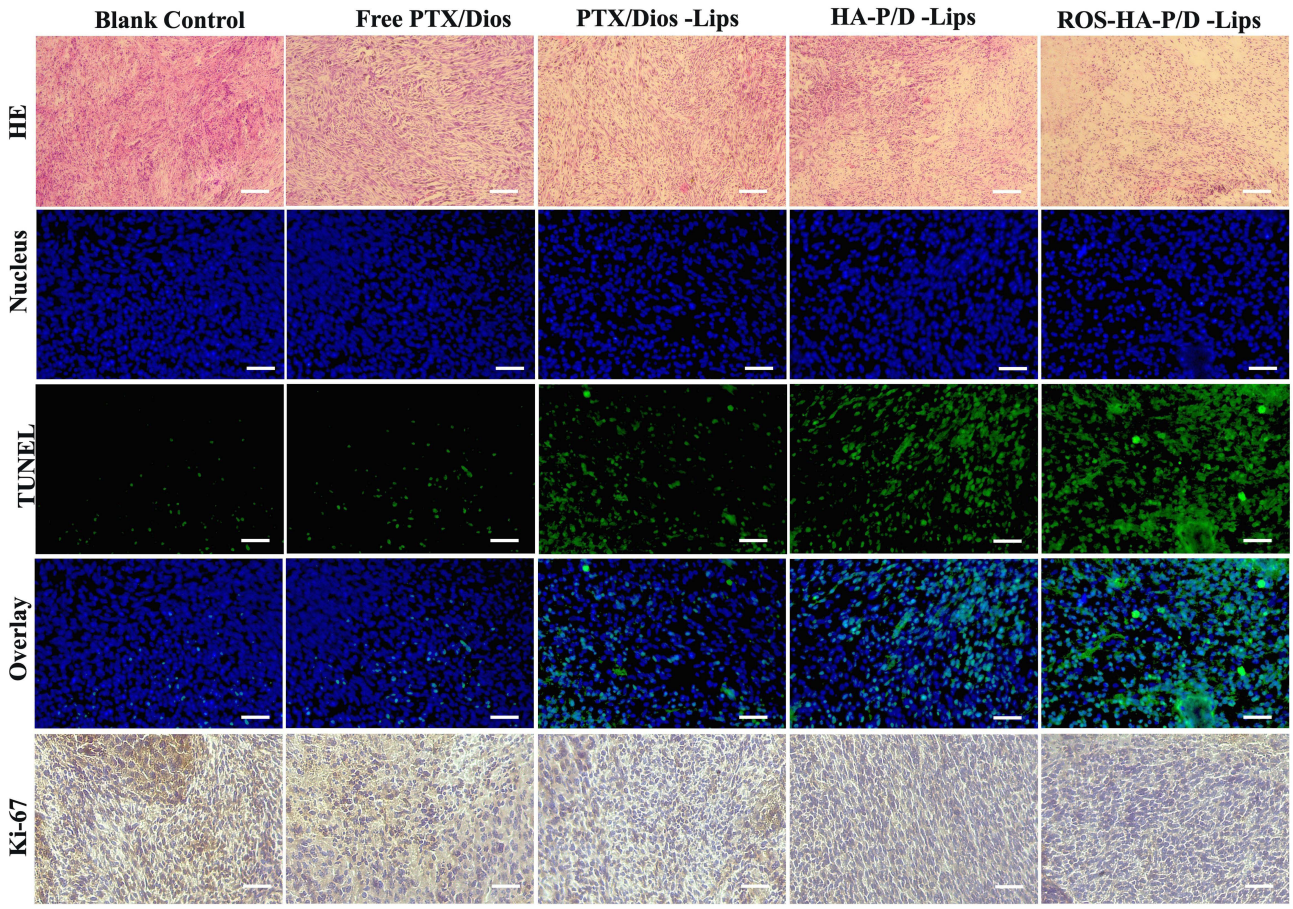

Figure 9 In vivo antitumor efficacy in tumor-bearing mice. (**A**) H&E staining of tumor tissue sections. (**B**) TUNEL staining. Positive staining indicates cell apoptosis. (**C**) Immunohistochemical staining of Ki-67 in tumor tissue. Scale bar, 25 μm.

in tumor tissues under the EPR effect. In addition, TEM images showed that PEG- TK-HA-PDLPs were spherical with a smooth surface, which could reduce the possibility of adhesion to the vascular endothelium (Figure 1E).

In cellular uptake experiments, we qualitatively and quantitatively compared the uptake of different agents by ID8 cells by fluorescence microscopy and flow cytometry. Both methods yielded consistent results, with a significant dose-dependent and time-dependent increase in cellular uptake of targeted liposomes (Figure 2). In addition, PEG-TK-HA-CLPs showed a weaker fluorescent signal in ID8 cells compared to HA-CLPs, which was due to the protection by the hydrophilic moiety DSPE-PEG_{2000}-TK-PEG_{5000}, and when this preparation was incubated with NaOH, the cleavable linker of TK was degraded, and the hydrophilic outer shell layer of the liposome's PEG disappeared, exposing the HA. Exposed HA significantly enhanced intracellular uptake through specific binding to CD44. Therefore, the targeted delivery system in this study not only has a PEG-mediated HA shielding effect to reduce nonspecific uptake, but also has ROS sensitivity (TK) to increase the penetration of antitumor drugs in TME. The results of stability experiments showed that the addition of TK increased the EE% and reduced the leakage of the drug, indicating a good protection of the drug, increased stability, and synergized the long drug cycle to achieve the EPR effect. In addition, in vitro release experiments showed that DSPE-PEG_{2000}-TK-PEG_{5000} protects HA-PDLPs to reach the tumor site in a ROS-responsive environment and then slowly releases the drug for better passive targeting.

The in vitro cytotoxicity profiles of different formulations on ID8 cells were investigated by SRB assay (Figure 4A and B). The results showed that the cytotoxicity of different liposome formulations on ID8 cells was ranked as PEG-TK-HA-PDLPs+NaOH > HA-PDLPs > PEG-TK-HA-PDLPs ≥ PDLPs > PLPs. Among these liposome formulations, the most pronounced cytotoxicity on ID8 cells was observed with PEG-TK-HA-PDLPs+NaOH, which indicated that after incubation with NaOH, ROS-responsive bonds were shed, and HA was exposed on the liposome surface, which enhanced

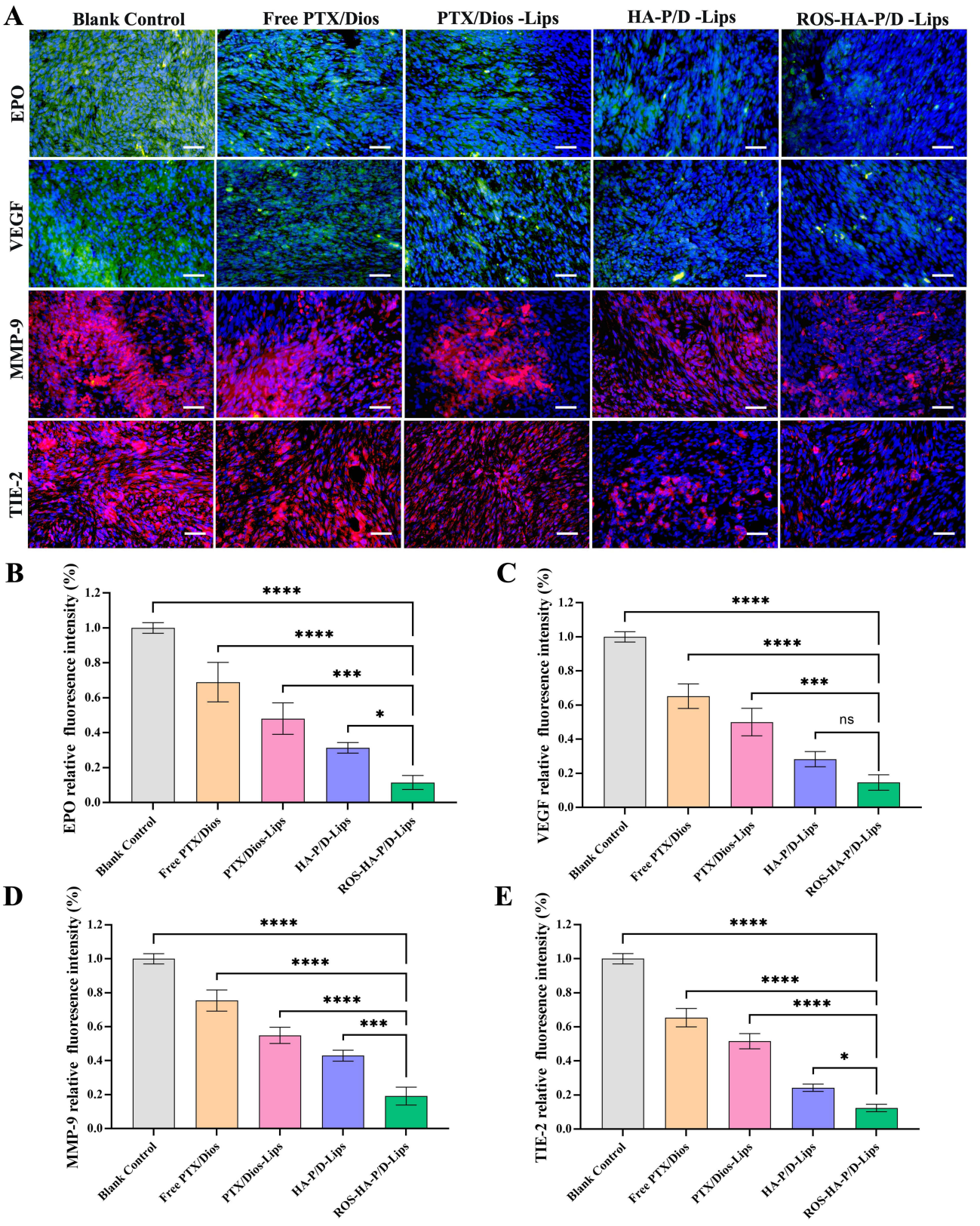

Figure 10 Inhibitory effects on tumor cell angiogenesis in tumor-bearing mice after treatment with various formulations. (**A**) Immunofluorescence detection of EPO, VEGF, MMP-9, and TIE-2. (**B**–**E**) EPO, VEGF, MMP-9, and TIE-2 were semi-quantitatively analyzed by relative fluorescence intensity. Scale bar, 25 μm. Data are presented as mean ± SD (n = 3), **P*<0.05, *** *P*<0.001, **** *P*<0.0001.

the cytotoxicity of the drug through active targeting. Figure 4D shows the results of live/dead cell staining. It was found that the ID8 cells in the control group were live cells with green fluorescence, while the HA-PDLPs and PEG-TK-HA-PDLPs+NaOH groups had the most severe cell death, which could effectively kill cancer cells. Synergy analysis using SynergyFinder showed that the two drugs, PTX and Dios, acted synergistically to enhance cytotoxicity, which is consistent with cytotoxicity results.

Apoptosis is a programmed cell death process that may occur in multicellular organisms and rarely occurs during cancer development. Tumor cell death driven by apoptosis and necrosis may enhance therapeutic efficacy. In this study, we first evaluated the proliferation of ID8 cells treated with different formulations. The results showed that HA-PDLPs and PEG-TK-HA-PDLPs+NaOH groups reduced the proliferation rate of EDU cells and significantly inhibited the growth of ID8 cells. Then, apoptosis was detected by Hoechst/PI double staining method for different formulations. The results also showed that HA-PDLPs and PEG-TK-HA-PDLPs induced the strongest apoptosis.

Tumor cell invasion and metastasis are important biological behaviors of tumor cells and the process of cancer metastasis to distant organs. However, cancer cells cannot accomplish this process alone. TME plays an important role in ovarian cancer cell metastasis by coordinating the behavior of tumor cells in various biological processes such as survival, proliferation, and migration, which is the key to peritoneal tumor dissemination.[23,35] The results of wound healing and Transwell invasion and migration assays showed that HA-PDLPs and PEG-TK-HA-PDLPs+NaOH groups could effectively inhibit the migration and invasion of ID8 cells.

To observe the real-time distribution and tumor-targeting ability of the different formulations, in vivo imaging was employed. The results showed that the fluorescent signals of PEG-TK-HA-DIR-LPs accumulated most strongly at the tumor site and could be maintained for 72 h. On the one hand, the hydrophilic PEG_{5000} formed a hydrated membrane on the liposome surface to protect HA to prolong the circulation time. On the other hand, the ROS-responsive polymer (TK) on the outermost side of the liposome is oxidized and decomposed to -SH, which exposes the targeting molecule HA and enhances the targeting activity accumulated at the tumor site.

In the safety inspection, there was no significant change in the body weight of tumor-bearing mice after treatment with PEG-TK-HA-PDLPs, and there was no significant damage to the organs of tumor-bearing mice stained with H&E, which indicated that the liposomes were safe (Figure 8A and D). Pharmacodynamic experiments showed that PEG-TK-HA-PDLPs significantly inhibited tumor growth (Figure 8B and C). Next, the enhanced antitumor effect of PEG-TK-HA-PDLPs was determined by H&E staining, TUNEL assay, and Ki-67 assay (Figure 9) in order to inhibit further tumor development and metastasis by damaging tumor tissues, inducing apoptosis, and inhibiting tumor cell proliferation. By providing oxygen, nutrients, and a conduit for metastasis, tumor angiogenesis is a crucial part of cancer metastasis.[36] Over the past decade, data from preclinical studies have shown that hypoxia-inducible erythropoietin (EPO) is not only a major regulator of erythropoiesis but is also a mutilative cytokine that also influences erythropoiesis in the formation of a cancer cell.[37] EPO stimulates the survival of cancer cells and has the ability to develop metastasis and drug resistance in cancer cell lines.[38] Vascular endothelial growth factor (VEGF) is one of the most common and important angiogenic pathways in OC, and its high level of expression indicates a poor prognosis.[39] Matrix metalloproteinases (MMPs), known to degrade extracellular matrix and basement matrix and basement membrane components, play important role in cancer invasion and metastasis.[40] MMPs are associated with OC, and clinical data show that MMP-9 expression levels are elevated in patients with ovarian cancer.[41] The literature suggests that monocyte endothelial cell-specific tyrosine kinase receptor (TIE-2), one of the monocyte subpopulations, plays a key role in tumor organization, tumor progression, and tumor spread.[42] Therefore, down-regulation of EPO, VEGF, MMP-9, and TIE-2 was necessary to inhibit angiogenesis. As shown in Figure 10, PEG-TK-HA-PDLPs downregulated the expression of angiogenesis-related proteins in vivo.

Conclusion

In this study, we constructed a ROS-responsive nanoparticle drug delivery system based on HA targeting CD44 for dual delivery of PTX and Dios and demonstrated that PEG-TK-HA-PDLPs could enhance antitumor efficacy in vitro and in vivo. As a multifunctional liposome, the excellent anti-tumor effect of PEG-TK-HA-PDLPs is mainly attributed to the following points: (i) the appropriate particle size of the liposome can increase the EPR effect, which can be enriched at the tumor site through passive targeting effect; (ii) The hydrophilic moiety DSPE-PEG_{2000}-TK-PEG_{5000} forms a hydrated

membrane on the surface of liposomes and protects the targeted ligand HA, thus preventing the non-specific uptake of HA into the cells and prolong their circulation time in vivo; (iii) TK cleavage between hydrophilic PEG_{5000} and nanocarrier cleaves and exposes HA in TEM, thereby enhancing active targeting; (iv) Encapsulation of PTX and Dios in liposomes enhances their bioavailability and effectively blocks tumor metastasis by inhibiting proliferation, angiogenesis and inducing apoptosis in OC cells. Therefore, PEG-TK-HA-PDLPs provide a novel strategy for the treatment of OC.

Funding

This work was supported by the National Natural Science Foundation of China (No. 81874347, 82204629).

Disclosure

The authors report no potential conflicts of interest in this work.

References

1. Howlader N, Cronin KA, Kurian AW, et al. Differences in breast cancer survival by molecular subtypes in the United States. *Cancer Epidemiol Biomarkers Prev*. 2018;27(6):619–626. doi:10.1158/1055-9965.EPI-17-0627
2. Siegel RL, Miller KD, Jemal A. Cancer statistics, 2020. *CA Cancer J Clin*. 2020;70(1):7–30. doi:10.3322/caac.21590
3. Wang ZB, Liu D, Lei G, et al. Editorial: ovarian cancer-targeted medication: PARP inhibitors, anti-angiogenic drugs, immunotherapy, and more. *Front Pharmacol*. 2023;14:1222209. doi:10.3389/fphar.2023.1222209
4. Califano D, Gallo D, Rampioni Vinciguerra G, et al. Evaluation of angiogenesis-related genes as prognostic biomarkers of bevacizumab treated ovarian cancer patients: results from the Phase IV MITO16A/Mango OV-2 Translational Study. *Cancers*. 2021;13(20):5152. doi:10.3390/cancers13205152
5. Morand S, Devanaboyina M, Staats H, et al. Ovarian cancer immunotherapy and personalized medicine. *Int J Mol Sci*. 2021;22(12):6532. doi:10.3390/ijms22126532
6. Penny SM. Ovarian cancer: an overview. *Radiol Technol*. 2020;91(6):561–575.
7. Lheureux S, Braunstein M, Oza AM. Epithelial ovarian cancer: evolution of management in the era of precision medicine. *CA Cancer J Clin*. 2019;69(4):280–304. doi:10.3322/caac.21559
8. Tian W, Lei N, Zhou J, et al. Extracellular vesicles in ovarian cancer chemoresistance, metastasis, and immune evasion. *Cell Death Dis*. 2022;13(1):64. doi:10.1038/s41419-022-04510-8
9. Wang YJ, Tang L, Lu XH, et al. Efficacy of epi-1 modified epirubicin and curcumin encapsulated liposomes targeting-EpCAM in the inhibition of epithelial ovarian cancer cells. *J Liposome Res*. 2023;33(2):197–213. doi:10.1080/08982104.2022.2153138
10. Ray U, Jung DB, Jin L, et al. Targeting LRRC15 inhibits metastatic dissemination of ovarian cancer. *Cancer Res*. 2022;82(6):1038–1054. doi:10.1158/0008-5472.CAN-21-0622
11. Jiang Y, Wang C, Zhou S. Targeting tumor microenvironment in ovarian cancer: premise and promise. *Biochim Biophys Acta Rev Cancer*. 2020;1873(2):188361. doi:10.1016/j.bbcan.2020.188361
12. Yeung TL, Leung CS, Yip KP, et al. Cellular and molecular processes in ovarian cancer metastasis. A review in the theme: cell and molecular processes in cancer metastasis. *Am J Physiol Cell Physiol*. 2015;309(7):C444–C456. doi:10.1152/ajpcell.00188.2015
13. Olmes GL, Breitbach GP, Tepikin A, et al. A metastasis of ovarian cancer in the bartholin gland: a case report with systematic literature review. *Reprod Sci*. 2023;31(2):550–554. doi:10.1007/s43032-023-01373-y
14. Taleb M, Ding Y, Wang B, et al. Dopamine delivery via pH-sensitive nanoparticles for tumor blood vessel normalization and an improved effect of cancer chemotherapeutic drugs. *Adv Healthc Mater*. 2019;8(18):e1900283. doi:10.1002/adhm.201900283
15. Zhang L, Zhang S, Jiang M, et al. Novel timosaponin aiii-based multifunctional liposomal delivery system for synergistic therapy against hepatocellular carcinoma cancer. *Int j Nanomed*. 2021;16:5531–5550. doi:10.2147/ijn.S313759
16. Zhang L, Kong L, He S, et al. The anti-ovarian cancer effect of RPV modified paclitaxel plus schisandra B liposomes in SK-OV-3 cells and tumor-bearing mice. *Life Sci*. 2021;285:120013. doi:10.1016/j.lfs.2021.120013
17. Li X, Wang J, Gu L, et al. Dual variable of drug loaded micelles in both particle and electrical charge on gastric cancer treatment. *J Drug Targeting*. 2020;28(10):1071–1084. doi:10.1080/1061186x.2020.1777419
18. Yang J, Shi X, Kuang Y, et al. Cell-nanocarrier drug delivery system: a promising strategy for cancer therapy. *Drug Deliv Transl Res*. 2023. doi:10.1007/s13346-023-01429-1
19. Banstola A, Poudel K, Pathak S, et al. Hypoxia-mediated ROS amplification triggers mitochondria-mediated apoptotic cell death via PD-L1/ROS-responsive, dual-targeted, drug-laden thioketal nanoparticles. *ACS Appl Mater Interfaces*. 2021;13(19):22955–22969. doi:10.1021/acsami.1c03594
20. Zhang YM, Xia M, Ao R, et al. Smart design of mitochondria-targeted and ROS-responsive CPI-613 delivery nanoplatform for bioenergetic pancreatic cancer therapy. *Nanomaterials*. 2021;11(11). doi:10.3390/nano11112875
21. Sun C, Liang Y, Hao N, et al. A ROS-responsive polymeric micelle with a pi-conjugated thioketal moiety for enhanced drug loading and efficient drug delivery. *Org Biomol Chem*. 2017;15(43):9176–9185. doi:10.1039/c7ob01975k
22. Wan WJ, Huang G, Wang Y, et al. Coadministration of iRGD peptide with ROS-sensitive nanoparticles co-delivering siFGL1 and siPD-L1 enhanced tumor immunotherapy. *Acta Biomater*. 2021;136:473–484. doi:10.1016/j.actbio.2021.09.040
23. Ween MP, Oehler MK, Ricciardelli C. Role of versican, hyaluronan and CD44 in ovarian cancer metastasis. *Int J Mol Sci*. 2011;12(2):1009–1029. doi:10.3390/ijms12021009

24. Zagorianakou N, Stefanou D, Makrydimas G, et al. CD44s expression, in benign, borderline and malignant tumors of ovarian surface epithelium. Correlation with p53, steroid receptor status, proliferative indices (PCNA, MIB1) and survival. *Anticancer Res*. 2004;24(3a):1665–1670.
25. Bayer IS. Hyaluronic acid and controlled release: a review. *Molecules*. 2020;25(11):2649. doi:10.3390/molecules25112649
26. Zhu L, Chen L. Progress in research on paclitaxel and tumor immunotherapy. *Cell Mol Biol Lett*. 2019;24(1):40. doi:10.1186/s11658-019-0164-y
27. Amaya C, Luo S, Baigorri J, et al. Exposure to low intensity ultrasound removes paclitaxel cytotoxicity in breast and ovarian cancer cells. *BMC Cancer*. 2021;21(1):981. doi:10.1186/s12885-021-08722-7
28. Kong L, Cai F, Yao X, et al. RPV-modified epirubicin and dioscin co-delivery liposomes suppress non-small cell lung cancer growth by limiting nutrition supply. *Cancer Sci*. 2020;111(2):621–636. doi:10.1111/cas.14256
29. Ikeda T, Ando J, Miyazono A, et al. Anti-herpes virus activity of Solanum steroidal glycosides. *Biol Pharm Bull*. 2000;23(3):363–364. doi:10.1248/bpb.23.363
30. Zheng L, Han X, Hu Y, et al. Dioscin ameliorates intestinal ischemia/reperfusion injury via adjusting miR-351-5p/MAPK13-mediated inflammation and apoptosis. *Pharmacol Res*. 2019;139:431–439. doi:10.1016/j.phrs.2018.11.040
31. Guo X, Ding X. Dioscin suppresses the viability of ovarian cancer cells by regulating the VEGFR2 and PI3K/AKT/MAPK signaling pathways. *Oncol Lett*. 2018;15(6):9537–9542. doi:10.3892/ol.2018.8454
32. Ledermann JA, Raja FA, Fotopoulou C, et al. Newly diagnosed and relapsed epithelial ovarian carcinoma: ESMO Clinical Practice Guidelines for diagnosis, treatment and follow-up. *Ann Oncol*. 2018;29(Suppl 4):iv259. doi:10.1093/annonc/mdy157
33. Patel A, Kalachand R, Busschots S, et al. Taxane monotherapy regimens for the treatment of recurrent epithelial ovarian cancer. *Cochrane Database Syst Rev*. 2022;7(7):CD008766. doi:10.1002/14651858.CD008766.pub3
34. Xu X, Saw PE, Tao W, et al. ROS-responsive polyprodrug nanoparticles for triggered drug delivery and effective cancer therapy. *Adv Mater*. 2017;29(33). doi:10.1002/adma.201700141
35. Ladoux B, Mege RM. Mechanobiology of collective cell behaviours. *Nat Rev Mol Cell Biol*. 2017;18(12):743–757. doi:10.1038/nrm.2017.98
36. He L, Zhu W, Chen Q, et al. Ovarian cancer cell-secreted exosomal miR-205 promotes metastasis by inducing angiogenesis. *Theranostics*. 2019;9(26):8206–8220. doi:10.7150/thno.37455
37. Szenajch JM, Synowiec AE. Erytropoetyna a lekoopornosc w raku piersi i raku jajnika [Erythropoietin and drug resistance in breast and ovarian cancers]. *Ginekol Pol*. 2016;87(4):300–304. Polish. doi:10.17772/gp/57817
38. Jeong JY, Feldman L, Solar P, et al. Characterization of erythropoietin receptor and erythropoietin expression and function in human ovarian cancer cells. *Int J Cancer*. 2008;122(2):274–280. doi:10.1002/ijc.23068
39. Jin C, Yuan M, Bu H, Jin C, Tomao F. Antiangiogenic strategies in epithelial ovarian cancer: mechanism, resistance, and combination therapy. *J Oncol*. 2022;2022:4880355. doi:10.1155/2022/4880355
40. Siu MKY, Jiang YX, Wang JJ, et al. Hexokinase 2 regulates ovarian cancer cell migration, invasion and stemness via FAK/ERK1/2/MMP9/NANOG/SOX9 signaling cascades. *Cancers*. 2019;11(6):813. doi:10.3390/cancers11060813
41. Liu H, Sun L, Liu X, et al. Associations between non-coding RNAs genetic polymorphisms with ovarian cancer risk: a systematic review and meta-analysis update with trial sequential analysis. *Medicine*. 2023;102(39):e35257. doi:10.1097/MD.0000000000035257
42. Turrini R, Pabois A, Xenarios I, et al. TIE-2 expressing monocytes in human cancers. *Oncoimmunology*. 2017;6(4):e1303585. doi:10.1080/2162402X.2017.1303585